Food Hydrocolloids 110 (2021) 106144

Contents lists available at ScienceDirect

Food Hydrocolloids

journal homepage: http://www.elsevier.com/locate/foodhyd

Comparative study of instrumental properties and sensory profiling of low-calorie chocolate containing hydrophobically modified inulin. Part II: Proton mobility, topological, tribological and dynamic sensory properties

Maryam Kiumarsi [a], Dorota Majchrzak [a], Henry Jäger [b], Jian Song [c], Oliver Lieleg [c], Mahdiyar Shahbazi [b,*]

[a] University of Vienna, Department of Nutritional Sciences, Faculty of Life Sciences, Althanstraße 14, A-1090, Vienna, Austria
[b] Institute of Food Technology, University of Natural Resources and Life Sciences (BOKU), Muthgasse 18, 1190, Vienna, Austria
[c] Department of Mechanical Engineering and Munich School of Bioengineering, Technical University of Munich, Boltzmannstraße 11, 85748, Garching, Germany

ARTICLE INFO

Keywords:
Surface-active biopolymer
NMR
Confocal Raman microscopy
Soft-tribology
Temporal Dominance of Sensations (TDS)
TDS difference curve

ABSTRACT

The aim of the present work was to evaluate the changes in instrumental measurements and dynamic sensory properties of chocolate as affected by the partial and total substitution of sucrose by dodecenyl-succinylated inulin upon storage. The results of textural, surface topology, and tribological properties of non-stored chocolates were found to be a function of modified inulin replacement, where an increase in modified inulin ratio allowed an increase in hardness, roughness, and friction coefficient. Compared to non-stored samples, the deterioration of textural properties after storage was inhibited in chocolate containing higher levels of modified inulin. Higher modified inulin ratios did not also induce an important change in NMR proton mobility, roughness, and friction coefficient upon storage. Confocal Raman microscopy revealed modified inulin located around sucrose and cocoa particles dispersed in fat phase, especially at the higher ratios. Temporal Dominance of Sensations (TDS) curves of non-stored samples elucidated that firmness was a dominant perception at the beginning of mastication, followed by melting rate, while cocoa flavor was experienced at the end of evaluation. However, these attributes were not perceived in stored chocolate with the lowest modified inulin. A PCA was performed to compare TDS scores and instrumental readings, showing a high correlation between instrumental measurement of hardness, friction coefficient, and NMR relaxation times and TDS score of firmness, bitterness, astringency, and melting rate. This work shows a new perspective to use biopolymeric surfactant for producing low-calorie chocolate, considering that hydrophobically modified inulin can diminish production costs and facilitate low-calorie product development.

1. Introduction

In recent years, there is an increased demand within the food industry for the production of free- and low-sugar products. The rise in cardiovascular disease, obesity, and other diet-related illnesses has led to consumers taking a greater interest to produce healthy, mainly low-sugar or sugar-free chocolates (Konar, Özhan, Artık, Dalabasmaz, & Poyrazoglu, 2014; Shah, Jones, & Vasiljevic, 2010). A technological resource for the development of low-calorie chocolate can be replacement of sucrose with low-calorie sweeteners. Inulin has been proved an attractive applicant as a bulking agent for low-calorie chocolate preparation (Afoakwa, Paterson, Fowler, & Vieira, 2009; Shah et al., 2010). It is of great interest to develop healthy products since it concurrently responds to various ranges of consumer requirements, i.e., it is fibre-enriched, prebiotic, low fat, and low sugar.

Many industrial formulations consist of dispersions of the suspensions or emulsions types. The stabilization of fat-based solid suspensions against phase separation requires the presence of an energy barrier between the particles that prevents their close approach, where the van der Waals attraction is large. Biopolymeric surfactants (i.e., surface-active biopolymers) are essential materials for the preparation of many disperse systems such as stabilization of fat-based suspension. It has been well recognized that graft biopolymeric surfactants behave in such a way that their hydrophobic portions interact mainly with the

* Corresponding author.
E-mail addresses: shahbazim00@yahoo.com, m.shahbazi1366@gmail.com (M. Shahbazi).

https://doi.org/10.1016/j.foodhyd.2020.106144
Received 13 March 2020; Received in revised form 21 June 2020; Accepted 28 June 2020
Available online 8 July 2020

hydrophobic phase, while their hydrophilic segments are disposed interacting mainly with the hydrophilic parts (Exerowa, Kolarov, Pigov, Levecke, & Tadros, 2006; Kokubun, Ratcliffe, & Williams, 2018; van Kempen, Schols, van der Linden, & Sagis, 2014). Recently, there has been substantial interest in the chemical and enzymatic modification of carbohydrate-based polymers to produce fatty acid ester derivatives as surface-active biopolymers, which have potential application to stabilize solid suspension (Kokubun et al., 2018; van Kempen et al., 2014). The production of low-cost and environmentally friendly biosurfactants is of practical interest due to economic, environmental, and health concerns about chemically synthesized surfactants. Biosurfactants have several advantages, such as low toxicity, biodegradability, production from renewable resources, and effectiveness under extreme conditions, and thus have attracted a great deal of attention for use as potential alternatives to the synthetic surfactants. These polymers have been reported to be effective in reducing surface tension and interfacial tension (Kiumarsi, Majchrzak, Yeganehzad, Jäger, & Shahbazi, 2020; van Kempen et al., 2014).

Inulin is an ideal candidate to be hydrophobically functionalized to obtain amphiphilic derivatives. The main advantages of hydrophobically modified inulin as a stabilizer for disperse systems are: (i) Strong adsorption to the particles through multi-point attachment with numerous alkyl chains. This ensures a lack of desorption and displacement of the molecule from the interface. (ii) Strong hydration of the linear polyfructose chains both in water and in the presence of high electrolyte concentrations and high temperatures. Several hydrophobic derivatives have been synthesized by the reaction of inulin in organic solvents with fatty acid chlorides, methyl esters, alkyl epoxides, and alkyl isocyanates (Exerowa et al., 2006; Khristov & Czarnecki, 2010). A 'green' method to modification has been introduced by Kokubun, Ratcliffe, and Williams (2015), Kokubun et al. (2018), and Kiumarsi et al. (2020), who have reported the modification of inulin using alkenyl succinic anhydrides. It has been shown that modification can be readily achieved by the interaction of inulin with alkenyl succinic anhydride in aqueous solution at room temperature, in which the products are surface-active and form micellar aggregates in solution.

So far there has been no study on the stabilization of a particle phase dispersed in a fat-based suspension (such as chocolate), using hydrophobically modified inulin, and most of the research works reported have involved the surface-active inulins for stabilization of the model emulsion. Moreover, there is no published report focusing on application of dodecenyl-modified inulin in the real food system. We have recently evaluated the functional properties of low-calorie chocolate formulated by dodecenyl-modified inulin, which presented good stabilizing properties and desired sensory attributes upon storage (Kiumarsi et al., 2020). Based on our findings reported in Part I of the present study, the produced low-calorie chocolates with intermediate and highest levels of modified inulin did not show any change in thermal behavior and crystalline patterns after three months of storage. Moreover, hydrophobically modified inulin at these levels led to the formation of a more stable system, and chocolates were free from any strong (irreversible) flocculation and coalescence. One noteworthy feature of modified inulin in the chocolate formulation is desired sensory attributes and offers greater stability against different storage conditions constituting an added value to the product at low concentrations. Therefore, graft copolymerization of inulin could be responsible for the stabilization properties of chocolate, which avoid destabilization and further phase separation of this product upon storage.

On the other hand, in Part I of this series, Quantitative Descriptive Analysis (QDA) as a static and single-point method was applied before the Temporal Dominance of Sensations (TDS), where TDS lexicon was easily derived from QDA (Kiumarsi et al., 2020). Using QDA and TDS together has been shown to be more beneficial than each just on its own. It is shown that those mean intensities provided by QDA cannot be used to predict the dominant sensations, as well as their temporal changes. Nevertheless, TDS only allows the evaluation of a limited number of attributes and so cannot replace QDA completely as subtle, less dominant; attributes may also contribute to product differentiation (Ng et al., 2012). Although the QDA and TDS methods display moderate comparability, the ability of the QDA methodology to determine a higher level of detail, as a result of the training in understanding a common lexicon, and subsequent alignment in the quantification of these attributes, more reveals the differences noted between methodologies. Indeed, the application of TDS to describe the sensory profile of products has been recognized as giving a different aspect of information to traditional descriptive analysis methodologies.

To extend our preceding work (Part I of this series), which described the stabilization features of chocolate formulated by dodecenyl-succinylated inulin, we evaluated mechanical assay, NMR proton mobility, internal distribution by confocal Raman microscopy, soft-tribological measurement and topological feature in both non-stored and stored chocolates to get more information on textural, morphological and structural properties. Then, the objectives of this study were to evaluate whether the previously reported stabilization effect, formation of the more stable system, and storage stability of biosurfactant-containing chocolates, described as an anti-blooming feature, are related to a network with a dense matrix structure and/or a decrease in oil migration. On the other hand, since limited research has applied the TDS methodology to chocolate and subsequently validated the results against QDA, another objective was to compare the results of TDS of low-calorie chocolates with the sensory profile obtained by QDA to understand if these methods can complement one another in profiling chocolates.

2. Materials and methods

2.1. Methods and materials

Materials have been described and characterized in detail in an earlier publication (Kiumarsi et al., 2020). Briefly, cocoa butter and cocoa powder were obtained from Guan Chong Cocoa Manufacture SDN (BHD, Malaysia). Soy lecithin was provided by (Lucas Meyer GmbH, Hamburg, Germany). Sugar powder was obtained from Sari Nira Nusantara CV (Yogyakarta, Indonesia). Inulin with an average DP $>$ 23 was purchased from Cosucra (FXL, Cosucra, Belgium) (details see Kiumarsi et al. (2020)).

2.2. Chocolate preparation

Low-calorie chocolates were prepared using the substitution of sugar by modified inulin as described in Part I of this series (Kiumarsi et al., 2020). Briefly, five batches (3 kg each) of chocolate were prepared by a similar method using the following formulation. The chocolates were prepared according to ingredients, including sucrose (25.7 wt%), cocoa butter (44.5 wt%), cocoa powder (29.7 wt%), and soy lecithin (0.1 wt %). Sucrose was replaced with different levels of dodecenyl-succinylated inulin (100:0, 75:25, 50:50, 25:75 and 0:100%) in chocolate formulation. The ingredients were then mixed in Vema mixer (Vema BM 30/20, Vemacon-struct, NV Machinery Verhoest, Izegem, Belgium) at a temperature of 45 °C and rotational speed of 5 rpm for 60 min. The chocolate samples were refined in semi-industrial production through a 3-roll refiner (Buhler Ltd., Uzwil, Switzerland) to a specified particle size of 20–35 μm. The refined chocolates were conched (IMC-E10, Mannhein, Germany) at 48 °C for 12 h, and finally tempered through a tempering machine (Hilliards Chocolate System, West Bridgewater, MA, USA). The tempered mass was molded into polycarbonate molds and allowed to cool in refrigerator (4 °C) for 30 min before de-molding. The final products were wrapped in aluminum foil and stored at 18 °C for further analysis. The codes of MI-25, MI-50, MI-75, and MI-100 were allocated to the chocolates with sucrose to modified inulin proportion of 75:25, 50:50, 25:75, and 0:100%, respectively.

2.3. Textural properties

Changes in chocolate formulation and storage condition affect the final chocolate quality like texture and durability (Afoakwa et al., 2009). Penetration test was conducted to obtain the mechanical parameters of chocolates using a texture analyzer (TA.XT-plus, Stable Micro Systems, Godalming, UK). Chocolate samples (40 × 50 × 10) mm^3 were penetrated by a flat stainless steel probe with a 5 mm diameter. Force calibration was carried out by using a 5 kg load cell to ensure maximal compression to shear ratio while maintaining enough contact surface between samples and probe. The obtained data were determined at a pre-speed of 0.5 mm s^{-1}, test speed of 1.5 mm s^{-1}, post-speed of 10 mm s^{-1}, and penetrating 5 mm at 18 °C. The textural parameters, including hardness (the point of maximum force needed for penetration) and fracturability (the point of the first peak or fracture), were calculated using Exponent Lite software (version 6.1.4, Stable Micro Systems, Godalming, UK) (Shahbazi, Rajabzadeh, Rafe, Ettelaie, & Ahmadi, 2017).

2.4. Surface topology

Topographic properties of chocolates were characterized by a digital instrument atomic force microscope (AFM, VEECO Dimension 3100, NY, USA) with Budget Sensors Tap300Al-G cantilevers. AFM operated at resonance frequencies of 350 kHz and tapping mode with a spring constant of 40 N m^{-1} resonance. A commercial etched silicon tip, as AFM probe, was used to analyze height and phase differences in samples. Chocolate samples were fixed onto a gently heated glass slide. The experiments were conducted at a temperature of 15 °C and relative humidity of (33.2 ± 1%). The scan size was set in the range of (50 × 50) μm^2 and was used for all roughness evaluations, which permitted suitable sampling and allowed for direct comparison of main surface properties. The roughness parameters, including average roughness (R_a) and root mean square roughness (R_q) were also obtained (Shahbazi, Majzoobi, & Farahnaky, 2018).

2.5. Proton nuclear magnetic resonance mobility

A low resolution (20 MHz) ^1H NMR spectrometer (MiniSpec mq 20 TD, Bruker, Rheinstetten, Germany) was employed to evaluate a wide range of proton molecular mobility and its distribution by measuring the free induction decay (FID), Carr-Purcell-Meiboom-Gill (CPMG) and transverse relaxation times. NMR device connected to a circulating water bath to keep the cell temperature at 18 °C. Chocolates were transferred into a 10 mm NMR tube. Then, T_2 spin-spin relaxation time was calculated from the FID profile using an inverse Laplace transformation through CONTIN application together with Minispec software (Bruker Corp., Germany). For FID sequence, an acquisition period of 0.5 μs was applied and 500 data points were collected. Regarding CPMG, the pulse lengths were obtained in 2.68 μs for the 90° pules and 5.24 μs for the 180° pulse, separating by an interpulse spacing of 0.1 ms, through which 2500 data points were obtained (Kiumarsi et al., 2019; Shahbazi, Jäger, Ahmadi, & Lacroix, 2020).

2.6. Confocal Raman microscopy

Confocal Raman microscopy was used to detect the component distribution within the chocolate matrix. The measurements were attained through a WITec alpha 300 RA+ system (Ulm, Germany) with a lateral resolution of 300 nm and 500 nm vertical resolution. A laser wavelength of 534 nm with a laser power of 15 mW was also used for the chocolates. Raman images were produced by taking 150 × 150 Raman spectra with a scan range of (50 × 50) μm^2. Before Raman imaging, chocolates were cut into 100-μm thick slices using a cryotome (Thermo Shandon, Waltham, MA, USA). A 65 × objective was used to view samples, and the integration time for each spectrum was 0.1 s. Further, the microscope was equipped with a Linkam cold stage set to 15 °C, preventing the chocolates from melting under the influence of the laser. Reference spectra were then recorded for cocoa butter, sucrose, cocoa powder, and modified inulin. Savitzky Golay smoothing was applied to all spectra, which decreased noise without any obvious loss of important information. To analyze the spectra and to make all the measurements and to create the Raman images, software program the WITec project 2.06 (Ulm, Germany) was employed. The chocolate spectra were fitted by a linear combination with the reference spectra in each pixel to obtain the relative occurrence of each component per pixel, from which an image was constructed based on the relative intensity of each component. The measured spectrum (S) is defined as:

$$S = (B \times h) + e \quad \text{Eq. (1)}$$

where, B is the matrix of the reference spectra of the components, h is the vector providing the fractions of the components, and e is the error spectrum. The mixing extents were fitted by the method of least squares minimizing the error as given in Eq. (2):

$$(e)^2 = \text{Minimum} \quad \text{Eq. (2)}$$

2.7. Dynamic sensory evaluation

Temporal Dominance of Sensations (TDS) method was applied to express differences in the dynamic sensory profile of chocolate variants. According to Pineau et al. (2009), the normalized time was plotted versus the dominance rate or selection frequency of each attribute at a specific point in time (%). Each curve showed the development of the dominance rate of an attribute over time. The chocolate samples were evaluated by ten trained panelists (5 males and 5 females, between 20 and 30 years of age). They were selected according to the guidelines of the ISO 8586:2012 standard (ISO, 2012) and acquainted with the attributes of chocolate. The following attributes involved in the analysis were determined through earlier assessments made by a focus group (Lawless & Heymann, 2010), including sweetness, sweet aftertaste, bitterness, bitter aftertaste, astringency, smoothness, firmness, powderiness, cocoa flavour, and melting rate. The references used to acquaint the panelists with the attributes of chocolate are shown in (Table A-1 in Supplementary Material). The assessors are asked to indicate which of the attributes is perceived as the dominant sensation, which is often defined as the most striking perception at a given time (Pineau et al., 2009).

After instructions were provided to the subjects, samples were presented to the sensory panel using a randomized complete block design in a monadic order (one-at-a-time) until all. Each panelist was asked to put a sample of chocolate (approximately 5 g) in their mouth and immediately start the evaluation. Then, they were requested to select the dominant sensory attribute that was experienced during the assessment. A 1-min break was provided between each evaluation to neutralize the mouth with unsalted crackers and tap water.

In the case of dynamic sensory properties, FIZZ software (Version 1.9) was used to compute the TDS curves and the chance and significance level were computed. For each product, the frequency of dominance of each attribute was established at each time point, with the subsequent outputs plotted against time, and smoothed by MATLAB (R2016a, MathWorks Inc., Natick, Ma, USA) to create TDS curves. To obtain an attribute picture of the development of dominant perceptions at the panel level, the sequences of each sensation were given and presented as TDS curves. Accordingly, standardized time (%) as x-axis was plotted against attribute dominance rates (DR%) as the y-axis and data smoothing was applied (Oberrauter, Januszewska, Schlich, & Majchrzak, 2018). Moreover, in order to facilitate the interpretation of TDS curves, two lines were displayed on each TDS graph, namely chance- and significance levels. The chance level represents the minimum value of a dominance rate that an attribute can obtain by chance (1/number of

attributes). The significance level specifies the minimum value of a dominance rate of a particular attribute that is significantly higher than the chance level ($P < 0.05$) (Pineau et al., 2009). TDS score was also taken into account as average intensity scores weighted by the duration of each selected attribute during the evaluation. This value was considered as the mean of the scores given to an attribute during an evaluation weighted by their duration. The TDS score for each attribute was determined as follows:

$$\text{TDS score} = \left(\sum_{\text{scoring}} \text{Intensity} \times \text{Duration}\right) / \left(\sum_{\text{scoring}} \text{Duration}\right) \quad \text{Eq. (3)}$$

2.8. TDS difference curve

In order to compare the impact of the storage condition for each sample, the normalized TDS difference curves regarding each attribute were plotted for each pair of samples (Pineau et al., 2009). The difference of the TDS curves was used to compare product pairs (i.e., non-stored vs. stored samples). As described by Pineau et al. (2009), TDS difference curves display the differences between dominance rates of attributes. These differences are plotted only when significantly different from zero, highlighting the differences between the products over time.

2.9. Tribology measurement

The tribological properties of the chocolate samples were examined using a steel-on-PDMS tribo-pairing. Steel balls with a diameter of 12.7 mm (Kugel Pompel, Vienna, Austria) were used as received. PDMS pins were prepared as cylinders with a diameter of 6.1 mm. In detail, PDMS prepolymer and cross-linker (Sylgard 184, Dow Corning, Wiesbaden, Germany) were mixed in a ratio of 10:1. Then, the mixture was placed into a vacuum chamber for 1 h to remove air bubbles. Afterward, the chocolates were poured into a steel mold and cured at 80 °C overnight. Both, the steel balls and PDMS pins were used without further polishing as they showed low roughness (Sqsteel < 200 nm, SqPDMS < 50 nm) when investigated with a laser scanning microscope (VK-X1100, Keyence, Osaka, Japan). The tribological measurements were conducted at 40 °C using the tribology unit (T-PTD 200, Anton Paar) of a commercial shear rheometer (MCR 302, Anton Paar) (Boettcher, Grumbein, Winkler, Nachtsheim, & Lieleg, 2014; Kiumarsi et al., 2019). In brief, three PDMS pins were mounted into a pin holder and washed with ethanol and ultrapure water. Then, ~600 μL of melted chocolate was applied to ensure full coverage of the pins. The normal load was chosen to be 6 N, resulting in average contact pressure of ~0.3 MPa. The sliding velocity was varied from 10^{-5} to 10 m s^{-1} to probe the tribological performance of the tested samples in a wide range of velocities. For each condition, three independent experiments were carried out using a fresh set of PDMS pins for each measurement.

2.10. Statistical analysis

All experiments were performed as triplicate determinations and the mean and standard deviation of the data were reported. Analysis of variance (ANOVA) was applied for the determination of the main effects of the investigated independent factors and their interactions on the instrumental and sensory data. Duncan's multiple range test was used to separate means of data when significant differences ($P < 0.05$) were observed (Majzoobi, Shahbazi, Farahnaky, Rezvani, & Schleining, 2013). Moreover, principal component analysis (PCA) was carried out by Unscrambler (Version 9.2, CAMO A/S, Oslo, Norway) to correlate data from TDS score and instrumental readings. PCA is used to identify or detect clusters in a data population in order to visualize the main variations in the data through principal components (PCs). The resulting score plot, where all samples are plotted according to the new coordinates from the transformed data, allows for easy interpretation of the main variation in the data set, and clusters of the samples are often visible using the first few PCs. A corresponding plot of variables (correlation loading plot) provides the correlations between the different variables.

3. Results and discussion

3.1. Textural characteristic

The results of the penetration test are summarized in Table 1. Textural data revealed that the non-stored control sample exhibited a significantly lower hardness ($P < 0.05$) than those formulated with dodecenyl-succinylated inulin. However, the hardness of chocolate including the lowest ratio of modified inulin was comparable to control, whose value was determined to be 6.24 N. Shah et al. (2010) and Konar et al. (2014) reported that incorporation of inulin at the lower content did not affect chocolate hardness. In the present study, sucrose replacement with modified inulin at the levels of 50, 75, and 100% effectively increased the hardness of non-stored control to 9.94, 10.82, and 14.51 N, respectively. This might be due to the denser network structure and greater complex modulus offered by the higher ratios of modified inulin (as shown in Part I of this series) (Kiumarsi et al., 2020). More solids packing density in low-calorie chocolate created strong interaction between particles, resulting in a higher maximum force required to penetrate the product. Likewise, the fracturability parameter of non-stored control sample from an initial value of 1.40 N was considerably increased to 3.61 N and 3.91 N after replacement of 50% and 75% modified inulin, respectively. As can also be seen in Table 1, the fracturability value was further increased by about 200% after total replacement of modified inulin. This could be correlated with the SEM findings described in part I of this study, in which a dense matrix with minimal inter-particle spaces was obtained at the higher concentrations of modified inulin (Kiumarsi et al., 2020). Therefore, the high solid packing density in chocolate structure develops strong interaction between particles, leading to a higher force required to fracture the product.

Table 1 also summarizes the hardness data of stored chocolates. The textural data revealed that hardness of stored control and MI-25 samples was higher than those of other samples. The observed textural changes were suspected to be caused by the restructuring and recrystallization of fat crystals in these chocolates, inducing blooming phenomena in the products, and thus increasing their hardness values. According to our previous study (Kiumarsi et al., 2020), a high frequency of fat crystal with rough surface was observed for stored control and MI-25. Afoakwa et al. (2009) also reported that blooming was initiated in stored chocolate causing a rapid increase in hardness, which attributed mainly to the growth of recrystallized fat within the chocolate network. In the present study, the hardness of MI-50, M-75, and MI-100 was unaffected over three months of storage and remained similar to those values obtained for the corresponded non-stored samples. It is reasonable to assume that during storage, grafted alkyl groups mostly interact with triglycerides in cocoa butter and the more polar central polymeric chain end interacting mostly with the surface of sucrose (or other hydrophilic domains), causing thus the necessary free energy reduction that avoids destabilization and further phase separation within chocolate suspension. Our previous work on the microstructure of low-calorie chocolate (Kiumarsi et al., 2020) showed that chocolates formulated with the higher contents of modified inulin were included more limited space and less crevices between particles with higher inter-particle network interaction. The presence of this dense structure was suspected to impede the movement of fat through the matrix onto the surface of the chocolate. Compared to non-stored chocolates, fracturability of stored control and MI-25 samples showed higher values, while fracturability of MI50, MI-75, and MI-100 did not change upon storage (Table 1). This might be also correlated with the results obtained from crystallography, where stable VI-type crystal was prevailing polymorphism in the stored

Table 1
The summary of textural properties obtained by penetration test and topological parameters measured by AFM for different chocolate samples.

Samples	Hardness (N)		Fracturability (N)		R_a[a] (μm)		R_q[b] (μm)	
	Non-stored	Stored	Non-stored	Stored	Non-stored	Stored	Non-stored	Stored
Control	6.21 ± 0.17[a]	16.41 ± 0.49[c]	1.40 ± 0.02[a]	4.77 ± 0.05[e]	20.3 ± 0.4[c]	59.3 ± 1.2[d]	31.2 ± 0.4[d]	74.1 ± 1.9[d]
MI-25	6.24 ± 0.13[a]	16.37 ± 0.34[c]	1.39 ± 0.02[a]	4.44 ± 0.07[d]	19.8 ± 0.3[c]	47.2 ± 0.9[c]	29.4 ± 0.6[c]	66.8 ± 1.4[c]
MI-50	9.94 ± 0.19[b]	10.09 ± 0.40[a]	3.61 ± 0.03[b]	3.71 ± 0.06[a]	11.5 ± 0.4[b]	12.6 ± 0.2[b]	22.0 ± 0.5[b]	23.1 ± 0.5[b]
MI-75	10.82 ± 0.24[c]	10.56 ± 0.33[a]	3.91 ± 0.02[c]	3.99 ± 0.04[b]	10.6 ± 0.2[a]	11.6 ± 0.4[a]	20.5 ± 0.5[a]	21.2 ± 0.6[a]
MI-100	14.51 ± 0.22[d]	14.45 ± 0.15[b]	4.22 ± 0.03[d]	4.30 ± 0.07[c]	11.7 ± 0.3[b]	12.9 ± 0.3[b]	22.8 ± 0.6[b]	24.0 ± 0.7[b]

[a–e] Means (three replicates) within each column with different letters are significantly different ($P < 0.05$), Duncan's test.
[a] R_a: Average roughness.
[b] R_q: Root-mean-square roughness.

control and MI-25. In contrast, stored MI-50, MI-75, and MI-100 presented desirable V-type polymorphism. Therefore, if sucrose is substituted with higher ratios of modified inulin in the chocolate formulation, the rapid deterioration of textural features during storage can be prevented.

3.2. AFM

The results of the three-dimensional AFM images are schematically shown in Fig. 1 and the average roughness (R_a) and root mean square roughness (R_q) of chocolate variants are also summarized in Table 1. The R_a expresses the average of the absolute value of height deviations from the mean surface, and R_q shows the extent of the root mean square average of height deviations from the mean plane. As visualized, the surface topography of non-stored control chocolate illustrated minor irregularity with some micro-sized particles on its surface, whose R_a and R_q values were determined to be 20.3 μm and 31.2 μm, respectively (Table 1). This slight uneven matrix could be related to the presence of low-level of soy lecithin used in the production of control chocolate, where VI-type fat crystal was almost abundant polymorphism in this sample (Kiumarsi et al., 2020). Similarly, non-stored chocolate with 25% modified inulin presented some small irregularities on its surface with a R_a and R_q of 19.8 μm and 29.4 μm, respectively. As expected, the surface topology of non-stored MI-50 (not shown), MI-75, and MI-100 presented almost even and homogeneous structure, without irregularities on their surfaces. In these samples, dodecenyl succinylated inulin at the intermediate and highest ratios acted as lubricant or surfactant, leading to desirable crystals (mainly V-type) and provided a network with a lower surface roughness (Table 1).

The AFM images clearly showed the storage condition had a remarkable impact on the surface topology of control and MI-25. As observed from Fig. 1, the changes in topographies of these samples over three months of storage were specified by a roughening of the surface, while phase imaging of other stored low-calorie chocolates showed no

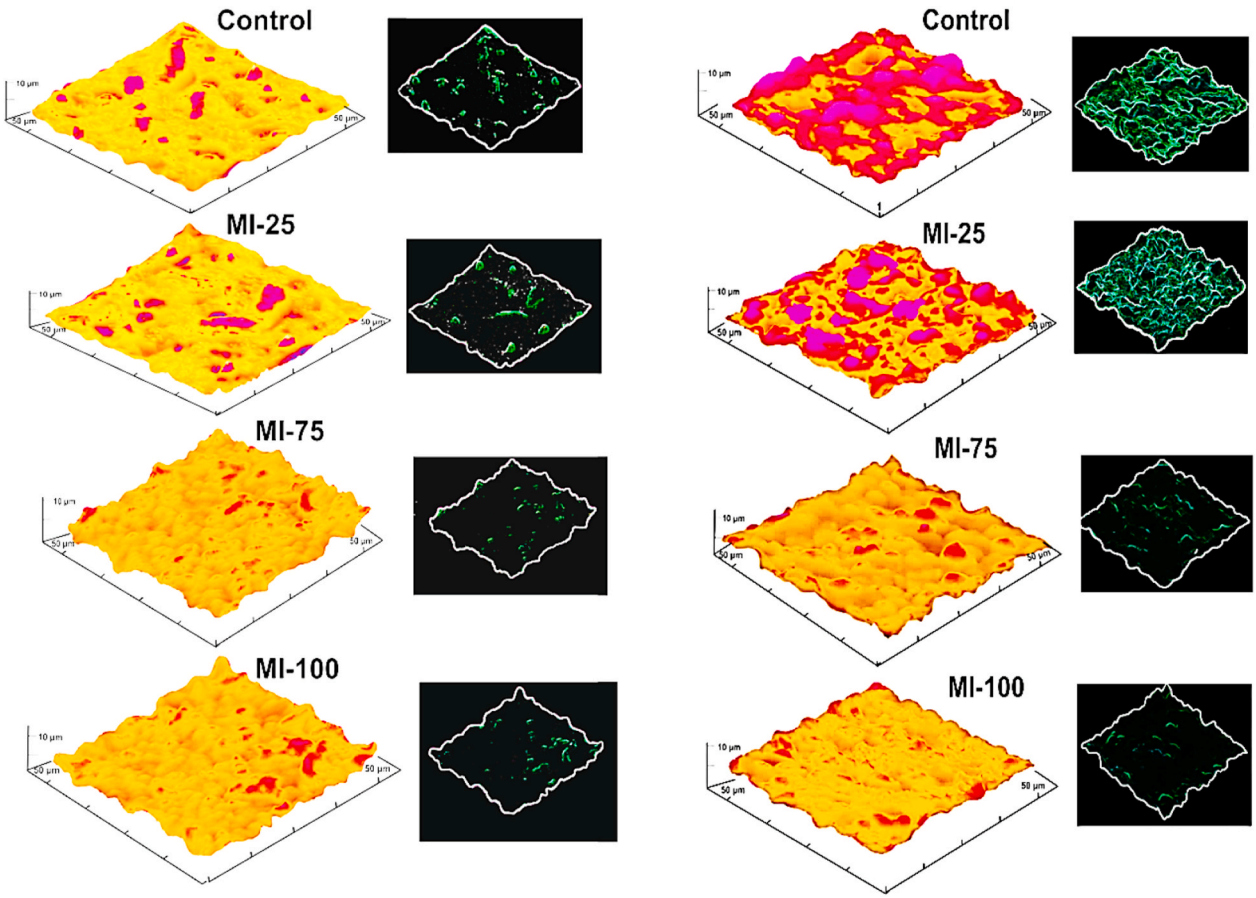

Fig. 1. Three-dimensional AFM micrographs of the surface of non-stored (left) and stored (right) chocolates. Scan size is (50 × 50) μm^2.

unexpected changes in contrast (Fig. 1). Generally, the stored control and MI-25 experienced a gradual increase in the crystal arrangement with many pits and hills on their surfaces with higher roughness parameters (Table 1), which reflected the effect of development of fat blooming. As mentioned earlier, gradual evolution of the polymorphic form VI was detected by DSC and XRD as the frequency of surface crystals was increased in the stored control and MI-25. The topographic information in the AFM images revealed the surfaces of MI-50 (not shown), MI-75, and MI-100 were still even and smooth upon storage with the areas of free slits and cracks or fat crystals.

3.3. NMR spectroscopy

Time-domain nuclear magnetic resonance (TD-NMR) has proven to be a quick, reproducible, accurate, and non-invasive technique, which is particularly well suited to oil mobility measurement. Fig. 2 displays the FID and CPMG proton distribution curves of chocolate as affected by modified inulin replacement and storage condition. The presence of two distinct FID and three CPMG proton populations was inferred from the relaxation signals of non-stored samples, specifying as $t_{(2,1)}$, $t_{(2,2)}$, $t_{(2,3)}$, $t_{(2,4)}$, and $t_{(2,5)}$ populations.

As can be seen in Fig. 2, two abundant proton populations were detected in the distribution patterns of non-stores samples. The first one (population $t_{(2,1)}$) appeared in the FID curve presented the lowest proton mobility, including solid fat crystals. The second dominant proton population (population $t_{(2,5)}$) was found in the CPMG peak, attributing to more mobile liquid oil. Solid fat crystals have been reported to present a relaxation time below 70 μs (Mansfield, 1971) and mobile oil shows T_2 relaxations greater than 2 ms (Duval, van Duynhoven, & Bot, 2006). Therefore, distinguished populations $t_{(2,1)}$ and $t_{(2,5)}$ could be assigned to fat crystals and free oil, respectively. NMR data revealed the proton distributions curves of non-stored control and MI-25 (curve not shown) samples were similar, not only in the resolution of the FID and CPMG spectra but also in the peak areas and in the relaxation time of population. As visualized from Fig. 2, the substitution of sugar by modified inulin in the non-stored MI-50-MI-100 caused a considerable increase in the amplitude of population $t_{(2,1)}$, being more pronounced when the highest ratio of modified inulin was used in the chocolate formulation. An increase in the peak area of population $t_{(2,1)}$ leads to an increase in the hardness of the system (Kiumarsi et al., 2019), which was in line with the textural observation of non-stored MI-50-MI-100 with higher hardness. According to the peak areas of the CPMG population, the abundant population $t_{(2,5)}$ was considerably decreased after the replacement of higher levels of modified inulin (Fig. 2). The lower peak area of $t_{(2,5)}$ relaxation in the cases of non-stored MI-50, MI-75, and MI-100 could be attributed to the decreased portions of more mobile oil. Since dodecenyl-succinylated inulin showed an oil-binding effect, it could decrease the amount of free oil in the system (Kiumarsi et al., 2020). Moreover, it might be due to increased interactions among molecules and presence of more crystalline material as more hydrophobic portions have interacted with the free oil in chocolate.

On the other hand, the replacement of sugar by higher contents of modified inulin exerted some changes in the T_2 relaxation time of non-stored chocolate. As summarized in Table 2, the T_2 relaxation time of populations $t_{(2,1)}$- $t_{(2,5)}$ in FID and CPMG was significantly shifted to the lower relaxations upon modified inulin replacement ($P < 0.05$), indicating the fact that the protons became less mobile and therefore, moved to the populations with shorter T_2 relaxation times. A shorter FID times is correlated with a high degree of crystallinity (Rogers, Wright, & Marangoni, 2008), which was in agreement with previously reported XRD and DSC results (Kiumarsi et al., 2020). This proposed the samples containing higher ratios of modified inulin have more functional groups available to entrap the oil, and accordingly the system requires less time to restore its initial spin orientation (Valoppi, Calligaris, & Marangoni, 2017).

NMR spectroscopy can also be used to study the change in the oil mobility inside chocolate matrix upon storage. The proton distribution patterns of stored chocolate variants are presented in Fig. 2. Using the

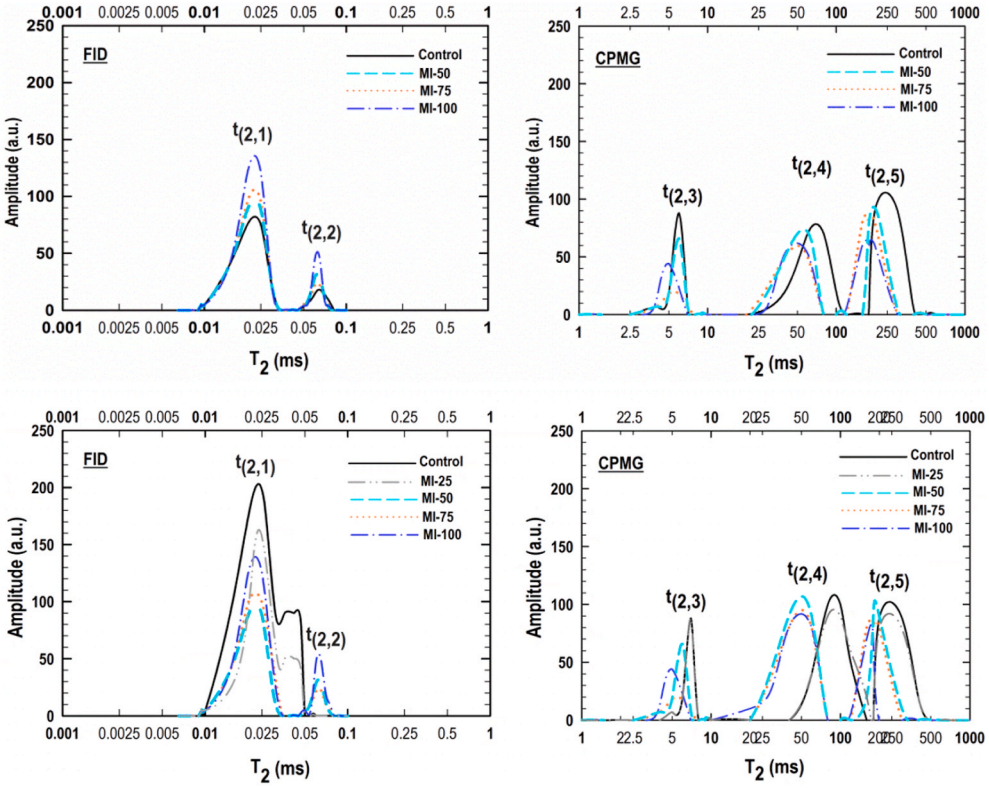

Fig. 2. Proton distributions of non-stored (up) and stored (down) chocolates determined by inverse Laplace transformation of the single pulse-free induction decay (FID) and of the decay obtained with the Carr-Purcell-Meiboom-Gill pulse sequence (CPMG).

Table 2
T_2 relaxation time of signal amplitude of protons detected by low-field ^{1}H NMR.

Samples	$t_{(2,1)} \times (10^{-3})$ (ms)		$t_{(2,2)} \times (10^{-3})$ (ms)		$t_{(2,3)}$ (ms)		$t_{(2,4)}$ (ms)		$t_{(2,5)}$ (ms)	
	Non-stored	Stored	Non-stored	Stored	Non-stored	Stored	Non-stored	Stored	Non-stored	Stored
Control	24±2^c	27±1^c	66±4^d	nd*	6.06±0.2^e	7.50±0.1^d	72.44±2.4^c	83.62±3.1^b	252±9^d	275±9^d
MI-25	24±3^c	27±1^c	66±6^d	nd	5.98±0.1^d	7.40±0.2^d	71.29±1.2^c	82.87±2.2^b	248±7^d	269±8^d
MI-50	22±1^b	21±1^b	64±6^b	65±5^b	5.77±0.1^c	5.71±0.1^c	51.97±1.9^b	50.75±1.7^a	195±6^c	199±8^c
MI-75	20±3^a	20±2^a	65±4^c	66±5^c	5.22±0.1^b	5.25±0.2^b	49.48±0.9^a	50.53±1.4^a	174±4^b	177±4^b
MI-100	20±2^a	21±1^b	62±3^a	63±2^a	4.90±0.1^a	4.92±0.2^a	49.28±1.2^a	50.45±0.8^a	161±7^a	165±3^a

$^{a–e}$ Values are the average of triplicates ± standard deviation. Different superscripts in each column show significant statistical difference ($P < 0.05$).
*nd: Not detected

FID pulse sequence, a remarkable increase in the amount of crystalline mass of stored control and MI-25 samples was inferred from the observed increases in the amplitude of T_2 signal. Besides, the $t_{(2,1)}$ proton distributions of stored control and MI-25 chocolates were considerably higher as compared to other samples. In these samples, the part of $t_{(2,2)}$ relaxation also became immobilized or entrained fat in $t_{(2,1)}$ proton population. An increase in signal amplitude upon storage indicated that the amount of crystalline mass increased in time, suggesting that crystallization was progressing upon storage due to the polymorphic transformation of crystalline domains. There was also a significant increase in the relaxation time of population $t_{(2,5)}$ in control and MI-25 upon storage compared to their non-stored counterparts (Table 2) ($P < 0.05$). This indicated that the proton mobility increased in stored control and MI-25, resulting in a loss in the suspension stability due to the entropic effects of a phase-separated system. In contrast, the proton distributions curves of stored MI-50, MI-75, and MI-100 were similar to their non-stored counterparts, not only in the resolution of the FID and CPMG spectra but also in peak areas and in the initial value of T_2 relaxation time of $t_{(2,1)}$-$t_{(2,5)}$ populations. Compared to stored control and MI-25, some higher proton mobility restriction in the stored MI-50, MI-75 and MI-100 detected as deduced from the shifting T_2 relaxation peak to the shorter times (Table 2). There was also no shift in the distribution of relaxations in time for stored MI-50-MI-100 in comparison with their related non-stored samples, suggesting that the oil mobility did not change during three months of storage. The process of stabilization might be ascribed to the fact that hydrophobically modified inulin coated the solid particles spreading into the lipid continuous phase producing a steric stabilization.

3.4. Confocal Raman microscopy

The internal distribution of chocolate constituents was mapped by the use of confocal Raman microscopy (CRM). The combination of Raman spectroscopy with confocal microscopic imaging is well-suited to detect the solid particles in a complex system as it provides label-free, non-invasive, in-situ visualization, micro-scale level, and high spatial resolution. Dynamic information provided by CRM can also form a linkage between the macro-level performance and the micro-level behaviors of chocolate components before and after storage to greatly enhance the mechanistic understanding (Dahlenborg, Millqvist-Fureby, Brandner, & Bergenstahl, 2012). Fig. 3 shows Raman reference spectra extracted for each of the main components, which were recorded to identify their distribution inside the system.

Assignments of the characteristic wavenumbers to molecular groups are also given in Table 3. The Raman spectra of sucrose showed bands of variable intensities mainly in the low wavenumber, ranging from 400 to 1400 cm^{-1}, and also some distinguished peaks in the high wavenumber range between 2710 and 2946 cm^{-1} and 3570 to 3512 cm^{-1}. Generally, the band at 422 cm^{-1} was assigned to the δ(C–C–O) ring vibration. The band at 544 cm^{-1} was related to α-glycosidic bond of C_1 on glucosyl subunit (Ilaslan, Boyaci, & Topcu, 2015). The two distinguished bands at 744 and 816 cm^{-1} were associated to the ν(C–C) vibration of

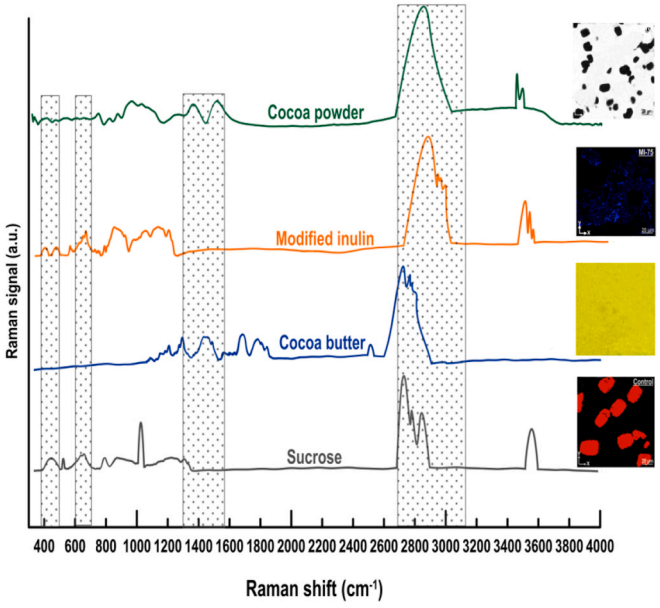

Fig. 3. Recorded reference spectra of sucrose, cocoa butter, modified inulin, and cocoa powder.

Table 3
Observed approximate frequencies (cm^{-1}) and assignments for Raman spectra of sucrose, cocoa powder, modified inulin, and cocoa butter.

Sucrose wavenumber (cm^{-1})	Modified inulin wavenumber (cm^{-1})	Cocoa powder wavenumber (cm^{-1})	Cocoa butter wavenumber (cm^{-1})	Assignment
3588–3612	3150–3600			**ν(OH)**
		3150–3600		**ν(NH)**
2712–2948	2794–3031	2830–3030	2606–2983	**ν(CH)**
		1664	1754–1859	**ν(C–O)**
		1645	1693	**ν(C–C)**
1467	1465	1579	1402–1509	**δ(CH_2)**
1244			1252–1309	**τ(CH_2)**
1079	1300–1420	1384		**δ(COH)**
	992–1254	1128		**ν(C–O)**
	923		1159–1204	**ν(C–C)**
		896		**ν(CNC)**
744, 816	723	797		**ν(C–C)**
544	551			**α-glycosidic**
422				**δ(C–C–O)**

ν: stretching mode, δ: bending mode, τ: twisting mode.

fructopyranose and fructofuranose, respectively. The distinct band at 1079 cm^{-1} was also associated with C–OH deformation. In the high wavenumber range of the spectra, there was ν(CH) hydrocarbon signal between 2712 and 2948 cm^{-1} and OH stretching relating hydroxyl groups with a sharp peak at 3588-3612 cm^{-1} (Dahlenborg et al., 2012;

Ilaslan et al., 2015).

Regarding cocoa butter, the prominent feature was ν(C–H) stretching region at a range of 2606–2983 cm^{-1}, with fewer intense bands at the lower frequencies. In this case, some bands appeared at 1754–1859 cm^{-1} (relating to ester carbonyl stretching region), 1693 cm^{-1} (assigning to the olefinic band), 1402–1509 cm^{-1} (corresponding to δ(CH_2) deformation region), 1252–1309 cm^{-1} (relating to τ(CH_2) twisting region) and 1159–1204 cm^{-1} (ν(C–C) skeletal modes). A similar result was previously reported by Bresson, Rousseau, Ghosh, Marssi, and Faivre. (2011). The modified inulin also presented some distinct bands in the low wavenumber range of the spectra. Deformation vibration of the glucose ring gives rise to a strong Raman band at 551 cm^{-1}. The spectral region between 723 and 1467 cm^{-1} in Raman spectra is dominated by the bands assigned to the bending vibrations of various groups like C–C bending, C–O stretching and C–H twisting mode from different rings. In the high wavenumber range of spectra, the bands ascribed to the symmetrical and asymmetrical stretching vibrations of the H–C–H appeared between 2794 cm^{-1} and 3031 cm^{-1}, respectively. The Raman features were also visible in the spectra of cocoa powder at 797, 896, 1128, and 1384 cm^{-1}. A band at 1579 cm^{-1} (corresponding to δ(CH_2) deformation region) was also observed in the Raman spectra. The spectra of cocoa powder also showed bands at 1664 (assigned to either C═C or C═O stretching modes) and 1645 cm^{-1} (assigned to a ring quadrant stretching mode).

Fig. 4 shows the location and distribution of dodecenyl-succinylated inulin in the chocolate samples before storage. As visualized, modified inulin distribution was clearly visible via CRM as a blue/bright blue color. Modified inulin in non-stored MI-25 appeared to be slightly distributed in the chocolate matrix. The non-stored MI-50 and MI-75 by contrast displayed a higher amount of dodecenyl-succinylated inulin dispersed throughout the entire system. This indicated that modified inulin at the intermediate contents was present in both the sucrose and lipid phases of chocolate as they could effectively coat the surfaces of solid particles dispersed in the fat phase. Finally, an even greater amount of dispersed modified inulin within the chocolate matrix could be observed for non-stored MI-100, surrounding a tightly dispersed in chocolate with minimal inter-particle spaces.

Confocal Raman horizontal scan of chocolates involving different components is shown in Fig. 5, which clearly shows that the sucrose, cocoa particles, and modified inulin were found within the fat matrix. The areas in the obtained scans represented fat-rich domains (yellow/bright yellow), sucrose-rich areas (red), modified inulin (green/bright green), and cocoa particles (black). The images showed quite well-dispersed particles in agreement with the impression from SEM images of chocolate published by Kiumarsi et al. (2020). A difference in dodecenyl-succinylated inulin distribution was evident between non-stored MI-25 and other inulin-added chocolates (Fig. 5). As specified, regarding non-stored MI-25, a small amount of modified inulin appeared to be only located within the lipid phase. In the case of non-stored MI-50 and MI-75 by contrast, modified inulin appeared to be uniformly well-distributed throughout the bulk, coating the solid particles. This proposed that the biopolymeric surfactant was present in both the sugar and lipid phases of the low-calorie chocolates. This also showed that the modified inulin at the higher ratios did not solely associate with the fat globules as they were also observed within the sugar phase as indicated by the confocal Raman image. Similarly, modified inulin in non-stored MI-100 appeared to be more evenly distributed into the system with the areas of free sucrose. Then, CRM represented that the addition of higher ratios of modified inulin in non-stored chocolates had a major influence on its distribution and location compared to the lowest ratio.

In contrast to the typical chocolate microstructure observed for non-stored samples, CRM images of stored control and MI-25 appeared quite different in structure (Fig. 5). In this regard, a notable increase in signal intensity of fat (yellow) and a loss in signals of sucrose and cocoa were observed for stored control and MI-25. A continuous fat phase was

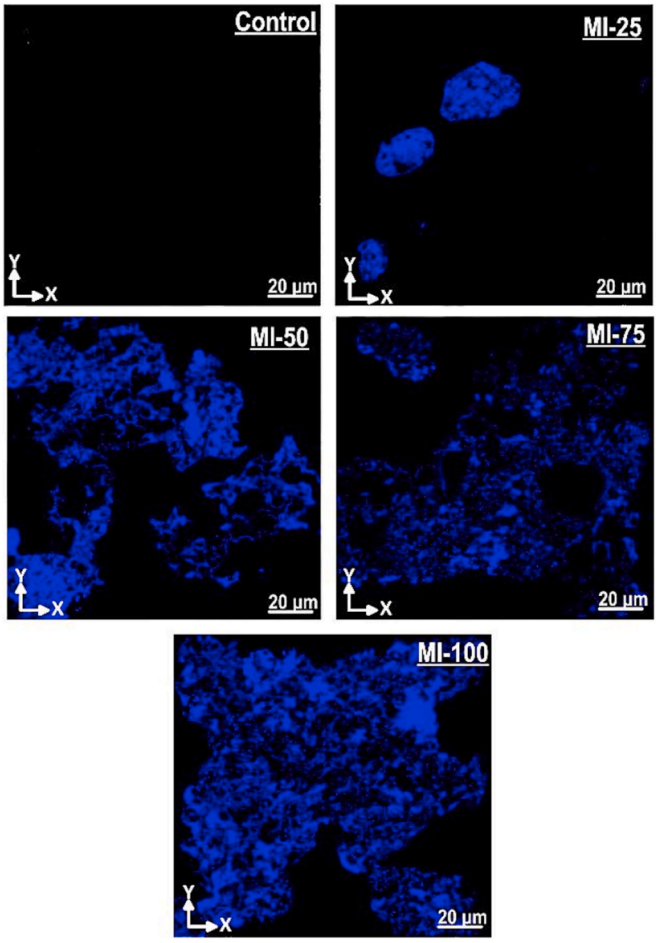

Fig. 4. Horizontal scans, *xy,* of the chocolate surface obtained from confocal Raman images, indicating the location and distribution of dodecenyl-succinylated inulin (blue/bright blue) in the matrix of non-stored samples. Scan range (50 × 50) μm^2 with 150 × 150 pixels in *xy*-direction, and penetration depth (focal plane) of 10 mm. (For interpretation of the references to color in this figure legend, the reader is referred to the Web version of this article.)

evident as an intense yellow color in the bulk, which was probably attributed to the presence of large crystallized aggregates of fat in these samples. The reason could be related to the development of blooming phenomena in the product upon storage. However, stored MI-50, MI-75, and MI-100, which contained higher ratios of modified inulin, did not show major microstructural changes, whose microstructures were almost similar to their corresponded non-stored samples. Minimal changes in microstructure over storage condition were expected because dodecenyl-succinylated inulin, as the biopolymeric surfactant, contributed to the stability of chocolate suspensions, improving the microstructure properties of the product in time; as it is very efficient in the term of steric stabilization owing to its molecular size and providing multiple binding sites at the interface. Owing to the importance of biopolymeric surfactant for the stabilization of solid particles in the fat-based food suspensions, the modified inulin contributes to the suspension stability against phase separation, where solid dispersion is free from any strong (irreversible) flocculation and coalescence. Then, the use of CRM proved to be a useful instrument in determining the distribution of modified inulin in low-calorie chocolates and would offer a sensitive analytical tool in future studies for observing specific chocolate components within the matrix throughout storage condition.

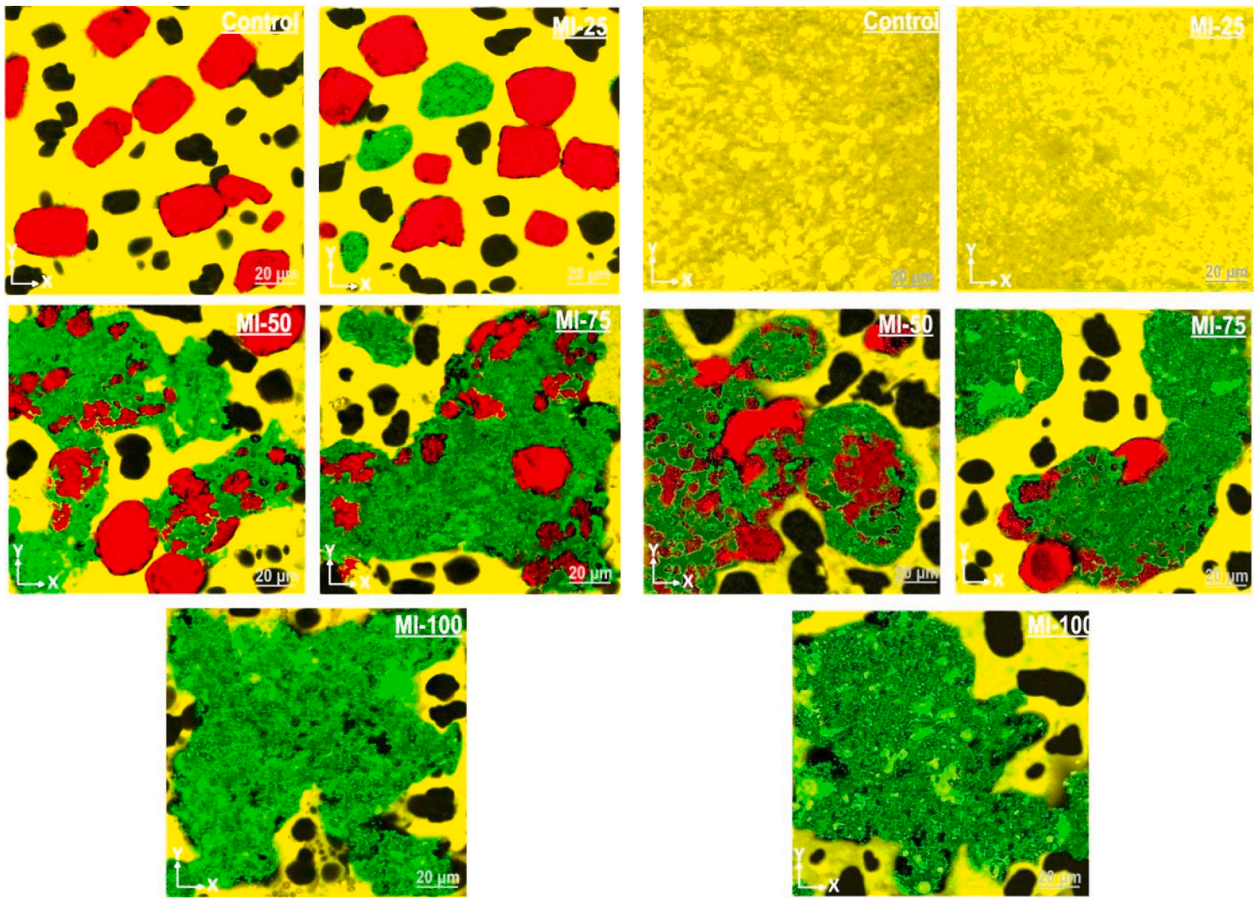

Fig. 5. Confocal Raman images indicating the different components in chocolate before (left) and after (right) storage condition. Red, black, yellow, and green colors specify sugar, cocoa, fat, and modified inulin, respectively. Scan range (50 × 50) μm^2 with 150 × 150 pixels in *xy*-direction, and penetration depth (focal plane) of 10 mm. (For interpretation of the references to color in this figure legend, the reader is referred to the Web version of this article.)

3.5. Dynamic sensory evaluation

The relationships between product-inherent characteristics, food structure, and consumer-related aspects (such as chewing pattern, efficiency, saliva flow rate, etc.) still need to be explored to systematically understand dynamic sensory evaluation. Fig. 6 displays TDS smooth curves for non-stored chocolates with a similar succession of dominant sensations in time with specific attributes appearing at the beginning, the middle, and the end of mastication. Each curve represents the development of the dominance rate of an attribute over standardized time (%). Based on the binomial distribution and considering ten attributes and 30 observations (10 assessors × 3 replicates), the critical values of the dominance rate (DR) for the significance of 95% and chance levels were determined to be 21% and 13%, respectively. In the temporal profile of all non-stored samples, firmness, melting rate, and cocoa flavor were perceived as a dominant attribute at the beginning, middle, and end of mastication, respectively. Moreover, the sweetness reached the level of significance only in non-stored control and MI-25 with a maximum dominance rate (max. DR%) of 40.5% and 39.1%, respectively, and for control lasted longer than MI-25. Furthermore, sweetness standardized time was delayed (about 12%) regarding non-stored MI-25 in comparison with control (Fig. 6). This difference could be related to the fact that modified inulin might have masked the sweet taste in MI-25 (Kiumarsi et al., 2019). In TDS curves of non-stored control and MI-25 chocolates, the sweet aftertaste was also the dominant sensation at the end of the evaluation and exceeded the significance level between the standardized time of about 63–76% of the evaluation period (control: max. DR = 28.7%; MI-25: max. DR = 27.4%). Compared to non-stored control and MI-25 samples, non-stored MI-50, MI-75, and MI-100 chocolates were dominated by firmness for a longer time and higher dominant rate, whose max. DR was determined to be 42.8%, 44.9%, and 48.2%, respectively. The high solids packing density in the chocolate formulation containing 50–100% dodecenyl-succinylated inulin could be resulted in a larger force required to chew the samples. The non-stored MI-50, MI-75, and MI-100 also experienced the greater dominance of the melting rate with max. DR of 38.1%, 39.5%, and 37.7%, respectively, dominating until the evaluation ended. This could be assigned to most desirable crystal form of fat in the chocolates formulated with higher ratios of modified inulin as shown by DSC and XRD experiments in Part I of this series (Kiumarsi et al., 2020). In this regard, form V was the most abundant polymorphism type in non-stored MI-50, MI-75, and MI-100, suggesting these variants showed better texture characteristics with a desirable melting behavior. As visualized from Fig. 6, bitterness dominated in non-stored MI-50 (max. DR = 22.3%), MI-75 (max. DR = 23.7%) and MI-100 (max. DR = 25.1%) for relatively short time at the middle of the mastication process. This fact might be due to the bitter taste of modified inulin at the higher concentration used in the chocolate formulation (Kiumarsi et al., 2020). The non-stored MI-100 was also dominated by a large proportion of perceived astringency (max. DR of 39.4%) almost along the entire evaluation period, proposing this attribute became more dominant when sugar totally was replaced by modified inulin. Moreover, this sample was characterized by a long-lasting bitter aftertaste, attaining max. DR of 28.3%.

On the other hand, the storage condition highly affected the dominance of the evaluated attributes in the control and MI-25 (Fig. 7). These cases could be mainly distinguished from the other chocolates by powderiness starting at the beginning of mastication as a dominant

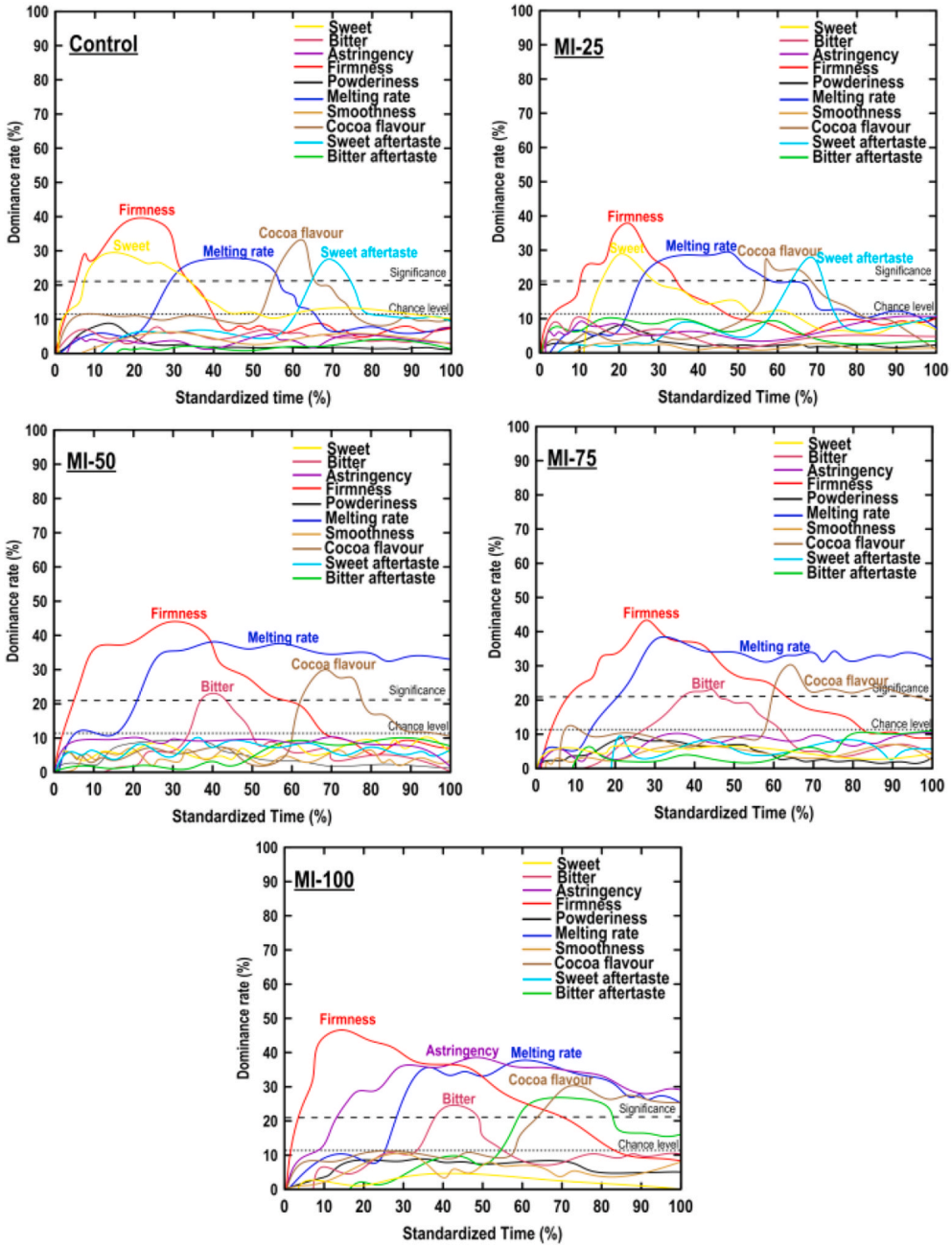

Fig. 6. Temporal profile of dominant sensations in standardized time with specific attributes in non-stored chocolate samples.

attribute and dominated during the entire evaluation period, as well as the sweet aftertaste, which dominated at the end of the evaluation. Regarding stored MI-25, bitter aftertaste also exceeded the level of significance from 58% up to 63% of evaluation period with max. DR of 29.8%. These results are in accordance with previous QDA reports about the influence of storage condition on control and MI-25 chocolates (Kiumarsi et al., 2020).

Compared to fresh control and MI-25, firmness, sweetness, melting rate, and cocoa flavor of stored control and MI-25 were not perceived as significantly dominant at any time of evaluation. This was consistent with the fact an increase in the frequency of surface fat crystals upon storage with the progress of blooming phenomenon. Fig. 7 also presents the TDS curves of the stored MI-50 and MI-75, which showed almost similar dominance profile compared to their non-stored counterparts, albeit with a lower max. DR% and shorter time of dominance above the significance level. In these cases, the TDS curves showed that firmness was still a significant dominant sensation at the beginning (max. DR = 35.4%), followed by the melting rate at the middle of the evaluation time (max. DR = 25.3%). As stated by Afoakwa (2016), good firmness and easy melting rate in the mouth are the main sensory texture attributes of chocolate on which the choice of consumers is based, giving a pleasant mouth-feel sensation. Compared to non-stored MI-50 (max. DR = 30.1%) and MI-75 (max. DR% = 29.6%), temporal perception of cocoa flavor for stored MI-50 (max. DR = 22.4%) and MI-75 (max. DR = 23.1%) was also found to be less dominant. Moreover, the temporal profile of stored MI-75 was distinguished from its non-stored counterpart, where bitterness significantly dominated at the middle of the testing period with max. DR of 21.9%. In the case of stored MI-100, a similar TDS profile was observed in comparison with non-stored MI-100, albeit with lower dominance rates. In this case, astringency was still approximately the dominant sensation nearly along the entire evaluation period (max. DR = 39.4%). A long-lasting bitter aftertaste was also

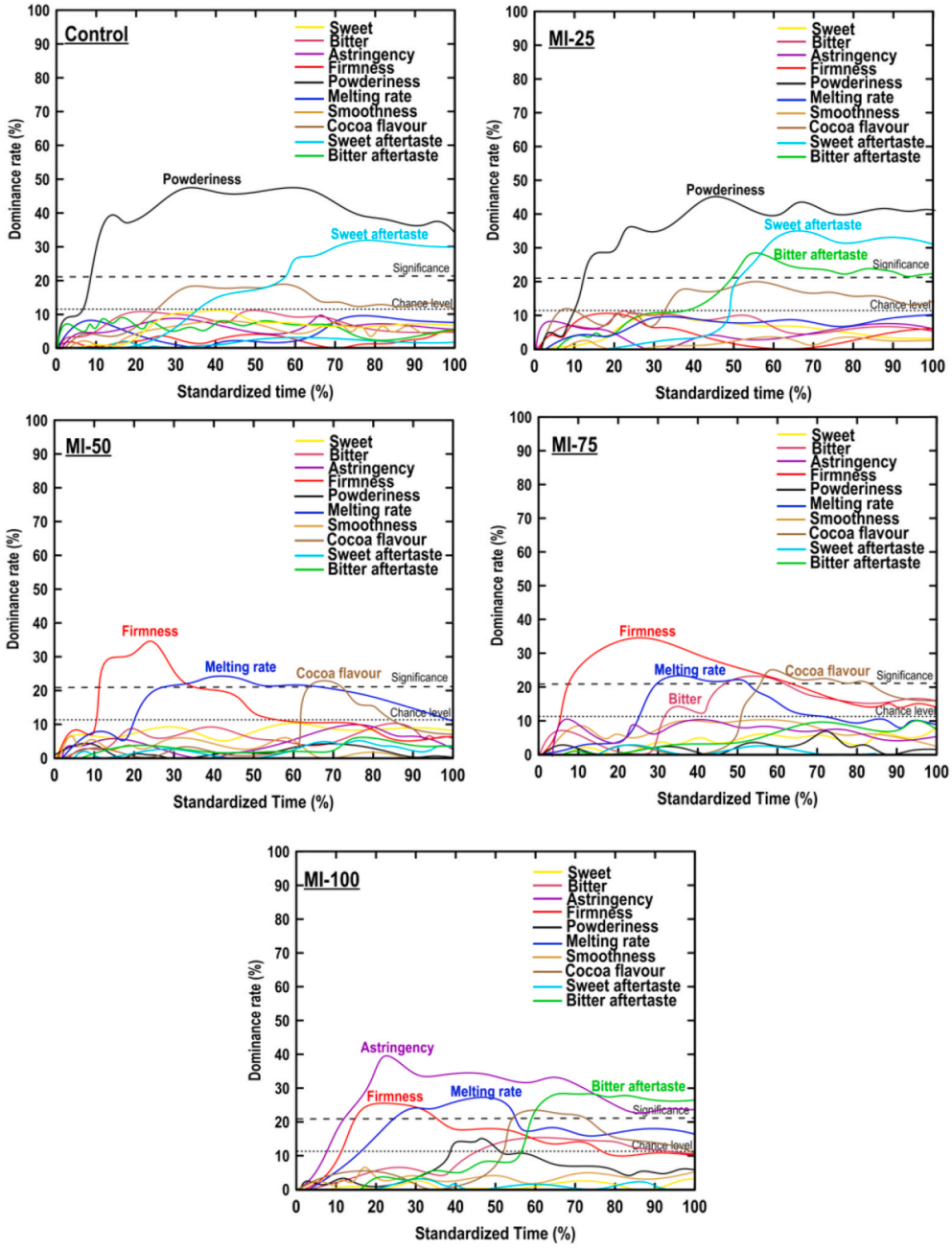

Fig. 7. Temporal profile of dominant sensations in standardized time in stored chocolate samples.

perceived significantly at the end of mastication, attaining the maximum dominance rate of DR = 29.1%. In general, stored samples containing intermediate and highest ratios of modified inulin showed similar dominance profiles when compared with their relevant non-stored counterparts. These observations agreed well with the QDA results reported in Part I (Kiumarsi et al., 2020). According to the TDS data, the replacement of sucrose by intermediate levels of modified inulin in chocolate is recommended with the purpose of long term storage, in which the stored chocolates presented a temporal profile similar to fresh variants.

One important aspect of the present work in the case of sensory evaluation was based on the selection of TDS attributes from QDA data according to findings described in Part I of the current study (Kiumarsi et al., 2020). The sensory sensations investigated in TDS could be selected from the list of the attributes generated during the training sessions of the QDA panel. TDS as a dynamic sensory method could be applied on key attributes to optimize the QDA protocol by indicating when these descriptors are more likely to be assessed correctly, on which time of mastication. For example, stored MI-100 was characterized by its unique bitterness distinguished in QDA, but TDS showed bitter taste only became dominant as aftertaste at the end of evaluation period (Fig. 7). In addition, stored control and MI-25 scored high in sweetness and sweet aftertaste intensity in QDA but were found to be dominated by sweet aftertaste instead of sweet taste with TDS. Compared to QDA, TDS curves showed that the smoothness attribute was not perceived as significantly dominant in both stored and non-stored samples. These results illustrated that the concept of dominance is independent of the concept of intensity, which agreed with the definition of the attribute dominance as given by Pineau and Schilch (2015). According to this, the dominant attribute is not the most intense descriptor, not the intensity that is the most prominent, but the attribute that attracts the most attention of the panelists. TDS works with several attributes, but it

focuses only on the dominance of the attributes over time and does not evaluate the intensity. However, the TDS score, which considers both the intensity and duration of dominance, is a measure of attribute intensity that can be compared to that obtained for the same attribute from QDA studies. TDS scores were evaluated by Eq. (3) from the TDS data, which were highly correlated to the QDA scores ($r \geq 95\%$, $P = 0.001$). When considering the product TDS score to the corresponding QDA profile data that almost all attributes were highly correlated between the two methods. However, upon correlating the results of TDS scores with the corresponding QDA profile ratings, the sweet and bitter aftertaste attributes were not correlated ($r < 44\%$, $P = 0.001$). This information showed that TDS could support the QDA for eight attributes perceived in the chocolates, which it should be considered as a complementary method for QDA. Moreover, the TDS scores were unable to distinguish the sensory appearance attributes evaluated by QDA, which was reported in Part I of this series (Kiumarsi et al., 2020). Then, QDA as a static and single-point method gave insight into many attributes that could be measured by TDS.

TDS difference curves comparing the dynamic sensory perception of chocolate as affected by storage condition are shown in Fig. 8. For control, the TDS difference curve showed that at the beginning of evaluation, the non-stored sample was perceived firmer and sweeter than the stored chocolate. In the middle of the process, the melting rate attribute was significantly more dominant. In contrast, powderiness was more dominant in the stored sample. A similar trend was observed for MI-25 (curve not shown). For MI-50 and MI-75, the dominance rate was significantly higher for the firmness in the non-stored samples than the stored samples at the beginning of the evaluation. In the middle of the evaluation, bitter attribute was significantly more dominant compared to stored chocolates. Regarding stored MI-50 and MI-75, cocoa flavor was significantly more dominant than non-stored samples. TDS difference curve of non-stored MI-100 showed a similar trend as that of MI-50 and MI-75 for firmness, bitterness, and cocoa flavor. On the opposite, stored MI-100 was mainly perceived as astringent in the middle of the process. It also highlights that the dominance rate was significantly higher for bitter aftertaste in stored MI-100 at the end of evaluation.

3.6. Soft-tribology measurement

If a suitable material pairing is used, tribological measurements can approximate the friction and lubricity behavior of products between oral surfaces. For example, soft-tribology measurements provide an insight into the tribological behavior of food during and following consumption, which in turn relates to their texture-related and mouthfeel sensory perceptions. Luengo, Tsuchiya, Heuberger, and Israelachvili (1997) studied the tribology of chocolate and related its lubrication behavior to the substitution of the continuous fat phase and the solid particles. They hypothesized that a strongly adsorbed hydrophobic monolayer was always present during sliding. This monolayer was suggested to lower the surface energy, thus changing the food texture at the interface by determining whether water, lipid, or other components are predominant at the interface. As illustrated in Fig. 9, both, non-stored control and

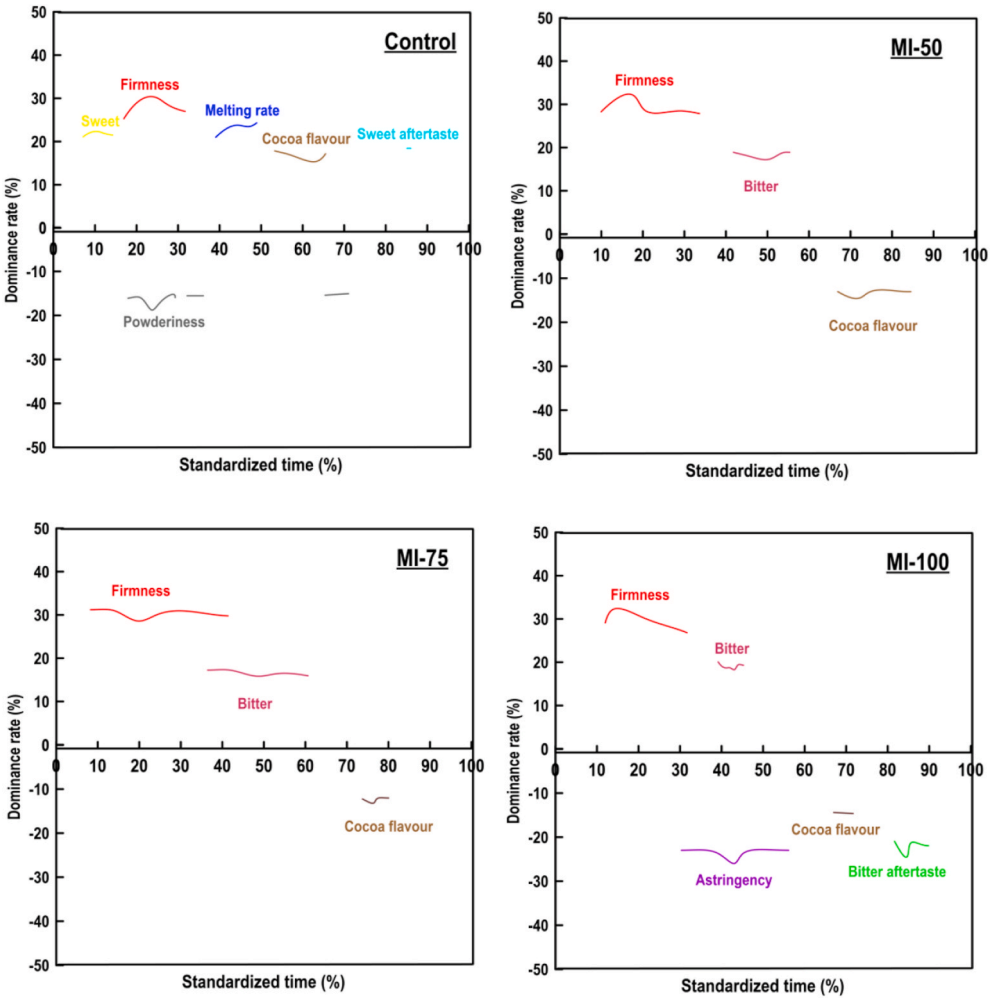

Fig. 8. Normalized TDS difference curves for each attribute and each pair of samples. The non-stored sample is always shown on top and stored chocolate in the bottom.

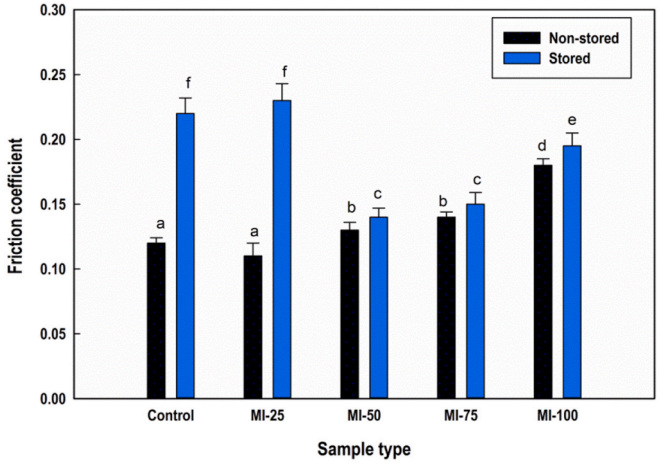

Fig. 9. Coefficient friction of chocolate determined by tribology as affected by the replacement of sugar by modified inulin and storage time. The sliding velocity was from 10^{-5} to 10 m s^{-1} at temperature of 40 °C.

MI-25 showed a lower coefficient of friction than the other non-stored chocolates. The SEM findings stated in Part I of this study (Kiumarsi et al., 2020) indicated that those samples exhibited a low solid packing density. Moreover, they showed lower values of roughness and NMR relaxation time (which, as mentioned earlier, is related to the hardness of a system). As expected, the friction coefficients obtained for non-stored MI-50, MI-75, and MI-100 chocolates gradually increased as a function of increasing the ratio of modified inulin to sugar. This is likely due to increased particle-particle interactions in the system and minimal inter-particle spaces, providing a harder matrix. This is proven that these chocolate variants could also be expected to trigger a different sensation in the oral cavity during chewing. Indeed, the tribological results are consistent with the sensory data obtained from TDS, where the firmness attribute was experienced as the dominant sensation for non-stored MI-50, MI-75, and MI-100. A simple Pearson's correlation analysis between variables proposed that the textural, topological, and NMR parameters were positively correlated with the measured friction coefficients. This Pearson's correlation analysis revealed that the measured friction coefficients were positively correlated with instrumental measurement of hardness (r = 0.92), fracturability (r = 0.89), R_a (r = 0.98), R_q (r = 0.97), $t_{(2,1)}$ relaxation time (r = 0.91) and $t_{(2,5)}$ relaxation time (r = 0.84) ($P < 0.05$), indicating that the friction coefficient may be an accurate predictor of these parameters. Moreover, a strong correlation with the TDS score of firmness (r = 0.91) was found ($P < 0.05$), i.e., an increase in friction was correlated with an increase in the force required to bite through the chocolate.

In the case of stored samples, control and MI-25 chocolates showed higher friction than their non-stored counterparts (Fig. 9). This effect might contribute to a grainy mouthfeel, and indeed, according to the TDS evaluation, these variants were predominantly perceived as 'powdery' almost during the entire evaluation period. In contrast, the replacement of sugar by 50%, 75%, and 100% modified inulin did not induce a significant change in the tribological properties of chocolate upon storage ($P > 0.05$), where stored MI-50, MI-75, and MI-100 samples were not perceived as predominantly powdery at any moment of consumption. Moreover, since certain rheological and tribological properties of a system are related to friction processes (Liu, Stieger, van der Linden, & van de Velde, 2015), occurring either internally (rheological) or at interfaces (tribological), a comparison of the results obtained from both rheological and tribological tests, may provide some insights into the fundamental relationship between those two properties. Our preceding study on rheological properties of low-calorie chocolate (Kiumarsi et al., 2020) revealed that a negligible sensitivity to the modified inulin content in the stored chocolates compared to non-stored ones at the intermediate and higher levels of modified inulin (50–100%). This suggested that the effect of modified inulin at these ratios on the tribological properties was primarily the result of the stability of chocolate suspensions and improvement in flow properties of stored products in the term of steric stabilization. This might be attributed to its surface-active functionality, in which there is an interaction between grafted alkyl groups on the inulin backbone with triglycerides in cocoa butter and polar central polymeric chain areas with sucrose (or other hydrophilic regions). As a result, the necessary free energy is reduced and destabilization and further phase separation of the suspension upon storage is avoided. Therefore, the replacement of intermediate and higher levels of modified inulin in chocolate will overcome the unfavorable grainy and powdery mouthfeel sensation. The tribological properties of the stored chocolates were also observed to be dependent on instrumental characteristics. Also here, a Pearson's correlation test indicated that the measured friction coefficients were positively related to the instrumental hardness (r = 0.95), fracturability (r = 0.86), R_a (r = 0.96), R_q (r = 0.96), $t_{(2,1)}$ relaxation time (r = 0.89), $t_{(2,5)}$ relaxation time (r = 0.81), and TDS score of firmness (r = 0.96) ($P < 0.05$). These results validated the use of tribology as an analytical method to better design products with specific sensory attributes.

3.7. Data mining with PCA

The resulting score plot is presented in Fig. 10a. The PC1 and PC2 explained 47.2% and 14.6% of the variation in the data set, respectively. The samples are separated into clusters related to the different treatments. The control and MI-25 formed a separate cluster on the PC-1 axis in the score plot compared to the other samples (Fig. 10a). The MI-50 is clustered in the left-hand side and the MI-100 in the right-hand side of the score plot, while the MI-75 overlaps between these two clusters.

The corresponding loading plot is shown in Fig. 10b. Variables located close to each other have a positive correlation, while variables with loadings of opposite signs are negatively correlated. The inner and outer circles mark the limits for 50% and 100% explanation of the variation in the data, respectively. The correlation loading plot (Fig. 10b) clearly displays that the variation along PC-1 is strongly influenced by instrumental characteristics of hardness, coefficient friction, amplitude $t_{(2,1)}$, amplitude $t_{(2,5)}$, T_2 $t_{(2,1)}$, T_2 $t_{(2,2)}$, and T_2 $t_{(2,5)}$ since these variables are localized between the inner and outer circles in the plot. The results from hardness, coefficient friction, T_2 $t_{(2,5)}$, and amplitude $t_{(2,1)}$ are placed close to each other to the right side of the plot, indicating a high correlation between these variables. Moreover, the PC1 clearly distinguished these parameters as opposed to T_2 $t_{(2,1)}$, T_2 $t_{(2,2)}$, and amplitude $t_{(2,5)}$ (to the left). The sensory assessments of firmness, bitterness, astringency, and melting rate are also localized in the same region of the correlation loading (to the right), indicating a positive correlation, while there is a negative correlation between these sensory attributes with perceived sweetness and sweet aftertaste.

The level of modified inulin in the chocolate formulation is also shown in the plot Fig. 10b by numbers corresponding to the ratio of modified inulin to sugar. The lowest ratio of modified inulin (25%) is located to the left side of the plot as opposed to the intermediate (50% and 75%) and highest ratios of modified inulin (100%). The PC1 thus also separates chocolates according to their formulation. The loading plot confirms that the chocolates with intermediate and highest ratios of modified inulin resulted in a high degree of hardness, coefficient friction, T_2 $t_{(2,5)}$, and amplitude $t_{(2,1)}$ as expected. On the other side of the plots, it is observed that chocolate with the lowest ratio of modified inulin is correlated with T_2 $t_{(2,1)}$, T_2 $t_{(2,2)}$, and amplitude $t_{(2,5)}$.

To be of value, instrumental readings need to be validated with sensory evaluations. Greater predictability of sensory analyzes by instrumental measurements translates into greater validity of instrumental characteristics. In the current study, a correlation between instrumental parameters and sensory evaluation was also performed (Fig. 10b). The instrumentally measured hardness is located next to the

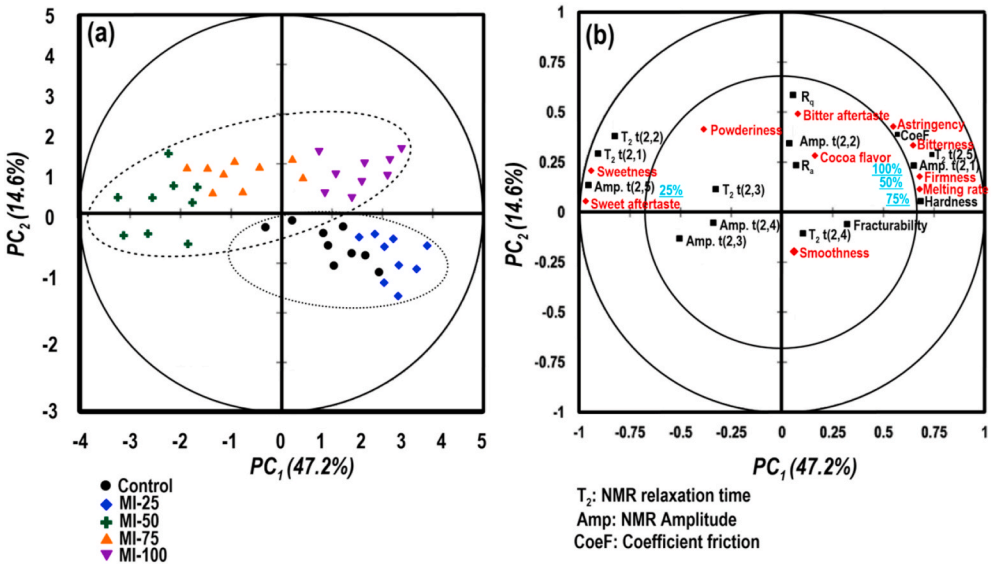

Fig. 10. Principal component analysis (PCA) of the results from all samples showing the first two principal components (PC1 and PC2). (a) Score plot showing all chocolates within each group, and the ellipses indicate clusters of the non-stored and stored groups in the experiment. (b) Correlation loading plot of the measured variables (▲ sensory attributes (TDS score), ■ instrumental measurements). The inner circle and the outer circle mark the limits for 50% and 100% explanation of the variation in the data, respectively. Explained variance for each PC is indicated on the axes.

sensory evaluation of firmness and on the opposite side of the plot compared to sensory evaluation of sweetness and sweet aftertaste. This indicates that hardness provides a good estimate of sensory firmness, sweetness, and sweet aftertaste of biosurfactant-containing chocolates. The sensory evaluations of bitterness and melting rate and instrumental measurements of hardness, coefficient friction, T_2 $t_{(2,5)}$, and amplitude $t_{(2,1)}$ are also localized in the same region of the correlation loading plot, indicating a positive correlation between these measurements, which supports the fact that higher levels of modified inulin would result in a higher bitterness and hardness. There is also a positive correlation between sensory properties of sweetness and sweet aftertaste with T_2 $t_{(2,1)}$, T $t_{(2,2)}$, and amplitude $t_{(2,5)}$.

4. Conclusion

The outcomes of the present study indicated the potential of using low-calorie chocolates formulated by dodecenyl-succinylated inulin and achieved the desired sensory attributes of chocolate after three months of storage. The results showed that the partial and total substitution of sucrose by dodecenyl-succinylated inulin in chocolate formulation had varied influences on the textural, tribological, structural, and morphological properties, as well as dynamic sensory features. By taking advantage of surface topology, proton mobility, and more specifically confocal Raman microscopy images, we were able to interpret the results of crystal growth, phase shift or separation, and anti-blooming effect of modified inulin upon storage. The images provided by confocal Raman microscopy also showed that the technique allows us to separate between the continuous fat matrix, sucrose particles, modified inulin, and cocoa particles. By comparing with the confocal Raman microscopy images of non-stored samples, the solid particles seemed to be more homogeneously distributed into the chocolate bulk in the case of stored chocolates with higher ratios of modified inulin. Stored chocolate with the lowest modified inulin ratio experienced instrumental or perceptual changes attributed to the storage condition, whose matrix was harder, more fracturable, and showed more amount of crystalline mass. In contrast, it could generally be observed that the functional properties of other samples with intermediate and highest modified inulin contents were unaffected over storage. Considering the dynamic phenomenon of oral processing, this study has contributed by taking into account the temporality of sensations during mastication by means of the TDS with a trained sensory panel and compared the results with the instrumental techniques. The sensory findings also indicated that the TDS methodology provides greater similarity to the QDA results on some of the key sensory attributes of chocolate. Then, this research identified the potential inclusion of TDS to complement the traditional QDA methodology, when specific information regarding the lingering profile of products is required. However, owing to the complexity of perceptions, additional studies should emphasis on aroma and flavor perception of low-calorie chocolates, in which further optimizing is necessary to attain chocolates with desirable sensory properties that would satisfy the acceptance of consumers.

Declaration of competing interest

The authors declare no conflict of interest.

CRediT authorship contribution statement

Maryam Kiumarsi: Investigation, Formal analysis. **Dorota Majchrzak:** Data curation, Supervision, Writing - review & editing. **Henry Jäger:** Writing - review & editing. **Jian Song:** Investigation, Formal analysis, Writing - review & editing. **Oliver Lieleg:** Methodology, Investigation, Writing - review & editing. **Mahdiyar Shahbazi:** Conceptualization, Methodology, Investigation, Validation, Funding acquisition, Writing - original draft, Writing - review & editing, Supervision.

Acknowledgement

The authors are grateful to Dr. Samira Yeganehzad from the Research Institute of Food Science and Technology (RIFST) for her helpful comments and guidance during the revision of this paper.

Appendix A. Supplementary data

Supplementary data to this article can be found online at https://doi.org/10.1016/j.foodhyd.2020.106144.

References

Afoakwa, E. O. (2016). *Chocolate science and technology*. John Wiley & Sons.

Afoakwa, E. O., Paterson, A., Fowler, M., & Vieira, J. (2009). Fat bloom development and structure-appearance relationships during storage of under-tempered dark chocolates. *Journal of Food Engineering, 91*(4), 571–581.

Boettcher, K., Grumbein, S., Winkler, U., Nachtsheim, J., & Lieleg, O. (2014). Adapting a commercial shear rheometer for applications in cartilage research. *Review of Scientific Instruments, 85*(9), Article 093903.

Bresson, S., Rousseau, D., Ghosh, S., Marssi, M. E., & Faivre, V. (2011). Raman spectroscopy of the polymorphic forms and liquid state of cocoa butter. *European Journal of Lipid Science and Technology, 113*(8), 992–1004.

Dahlenborg, H., Millqvist-Fureby, A., Brandner, B. D., & Bergenstahl, B. (2012). Study of the porous structure of white chocolate by confocal Raman microscopy. *European Journal of Lipid Science and Technology, 114*(8), 919–926.

Duval, F. P., van Duynhoven, J. P., & Bot, A. (2006). Practical implications of the phase-compositional assessment of lipid-based food products by time-domain NMR. *Journal of the American Oil Chemists Society, 83*(11), 905–912.

Exerowa, D., Kolarov, T., Pigov, I., Levecke, B., & Tadros, T. (2006). Interaction forces in thin liquid films stabilized by hydrophobically modified inulin polymeric surfactant. 1. Foam films. *Langmuir, 22*(11), 5013–5017.

Ilaslan, K., Boyaci, I. H., & Topcu, A. (2015). Rapid analysis of glucose, fructose and sucrose contents of commercial soft drinks using Raman spectroscopy. *Food Control, 48*, 56–61.

ISO (International Organization for Standardization). (2012). *ISO 8586. Sensory analysis: General guidelines for the selection, training and monitoring of selected assessors and expert sensory assessors*.

van Kempen, S. E., Schols, H. A., van der Linden, E., & Sagis, L. M. (2014). Effect of variations in the fatty acid chain on functional properties of oligofructose fatty acid esters. *Food Hydrocolloids, 40*, 22–29.

Khristov, K., & Czarnecki, J. (2010). Emulsion films stabilized by natural and polymeric surfactants. *Current Opinion in Colloid & Interface Science, 15*(5), 324–329.

Kiumarsi, M., Majchrzak, D., Yeganehzad, S., Jäger, H., & Shahbazi, M. (2020). Comparative study of instrumental properties and sensory profiling of low-calorie chocolate containing hydrophobically modified inulin. Part 1: Rheological, thermal, structural and external preference mapping. *Food Hydrocolloids*, 105698.

Kiumarsi, M., Shahbazi, M., Yeganehzad, S., Majchrzak, D., Lieleg, O., & Winkeljann, B. (2019). Relation between structural, mechanical and sensory properties of gluten-free bread as affected by modified dietary fibers. *Food Chemistry, 277*, 664–673.

Kokubun, S., Ratcliffe, I., & Williams, P. A. (2015). The emulsification properties of octenyl-and dodecenyl-succinylated inulins. *Food Hydrocolloids, 50*, 145–149.

Kokubun, S., Ratcliffe, I., & Williams, P. A. (2018). The interfacial, emulsification and encapsulation properties of hydrophobically modified inulin. *Carbohydrate Polymers, 194*, 18–23.

Konar, N., Özhan, B., Artık, N., Dalabasmaz, S., & Poyrazoglu, E. S. (2014). Rheological and physical properties of inulin-containing milk chocolate prepared at different process conditions. *CyTA - Journal of Food, 12*(1), 55–64.

Lawless, H. T., & Heymann, H. (2010). *Sensory evaluation of food: Principles and practices*. Springer Science & Business Media.

Liu, K., Stieger, M., van der Linden, E., & van de Velde, F. (2015). Fat droplet characteristics affect rheological, tribological and sensory properties of food gels. *Food Hydrocolloids, 44*, 244–259.

Luengo, G., Tsuchiya, M., Heuberger, M., & Israelachvili, J. (1997). Thin film rheology and tribology of chocolate. *Journal of Food Science, 62*(4), 767–812.

Majzoobi, M., Shahbazi, M., Farahnaky, A., Rezvani, E., & Schleining, G. (2013). Effects of high pressure homogenization on the physicochemical properties of corn starch. In *Inside Food symposium* (pp. 33–35).

Mansfield, P. (1971). Symmetrized pulse sequences in high resolution NMR in solids. *Journal of Physics C: Solid State Physics, 4*(11), 1444.

Ng, M., Lawlor, J. B., Chandra, S., Chaya, C., Hewson, L., & Hort, J. (2012). Using quantitative descriptive analysis and temporal dominance of sensations analysis as complementary methods for profiling commercial blackcurrant squashes. *Food Quality and Preference, 25*(2), 121–134.

Oberrauter, L. M., Januszewska, R., Schlich, P., & Majchrzak, D. (2018). Sensory evaluation of dark origin and non-origin chocolates applying Temporal Dominance of Sensations (TDS). *Food Research International, 111*, 39–49.

Pineau, N., & Schilch, P. (2015). Temporal dominance of sensations (TDS) as a sensory profiling technique. In *Rapid sensory profiling techniques* (pp. 269–306). Woodhead Publishing.

Pineau, N., Schlich, P., Cordelle, S., Mathonnière, C., Issanchou, S., Imbert, A., et al. (2009). Temporal Dominance of Sensations: Construction of the TDS curves and comparison with time–intensity. *Food Quality and Preference, 20*(6), 450–455.

Rogers, M. A., Wright, A. J., & Marangoni, A. G. (2008). Crystalline stability of self-assembled fibrillar networks of 12-hydroxystearic acid in edible oils. *Food Research International, 41*(10), 1026–1034.

Shahbazi, M., Jäger, H., Ahmadi, S. J., & Lacroix, M. (2020). Electron beam crosslinking of alginate/nanoclay ink to improve functional properties of 3D printed hydrogel for removing heavy metal ions. *Carbohydrate Polymers*, 116211.

Shahbazi, M., Majzoobi, M., & Farahnaky, A. (2018). Physical modification of starch by high-pressure homogenization for improving functional properties of κ-carrageenan/starch blend film. *Food Hydrocolloids, 85*, 204–214.

Shahbazi, M., Rajabzadeh, G., Rafe, A., Ettelaie, R., & Ahmadi, S. J. (2017). Physico-mechanical and structural characteristics of blend film of poly (vinyl alcohol) with biodegradable polymers as affected by disorder-to-order conformational transition. *Food Hydrocolloids, 71*, 259–269.

Shah, A. B., Jones, G. P., & Vasiljevic, T. (2010). Sucrose-free chocolate sweetened with Stevia rebaudiana extract and containing different bulking agents–effects on physicochemical and sensory properties. *International Journal of Food Science and Technology, 45*(7), 1426–1435.

Valoppi, F., Calligaris, S., & Marangoni, A. G. (2017). Structure and physical properties of oleogels containing peanut oil and saturated fatty alcohols. *European Journal of Lipid Science and Technology, 119*(5), 1600252.